

TUMOR IMMUNOLOGY

Contribution of resident and circulating precursors to tumor-infiltrating CD8⁺ T cell populations in lung cancer

Paul Gueguen^{1*}, Christina Metoikidou^{1*}, Thomas Dupic^{2†}, Myriam Lawand^{1†}, Christel Goudot¹, Sylvain Baulande³, Sonia Lameiras³, Olivier Lantz^{1,4}, Nicolas Girard⁵, Agathe Seguin-Givelet^{6,7}, Marine Lefevre⁶, Thierry Mora⁸, Aleksandra M. Walczak⁹, Joshua J. Waterfall^{10,11§}, Sebastian Amigorena^{1‡§}

Copyright © 2021
The Authors, some
rights reserved;
exclusive licensee
American Association
for the Advancement
of Science. No claim
to original U.S.
Government Works

Tumor-infiltrating lymphocytes (TILs), in general, and especially CD8⁺ TILs, represent a favorable prognostic factor in non-small cell lung cancer (NSCLC). The tissue origin, regenerative capacities, and differentiation pathways of TIL subpopulations remain poorly understood. Using a combination of single-cell RNA and T cell receptor (TCR) sequencing, we investigate the functional organization of TIL populations in primary NSCLC. We identify two CD8⁺ TIL subpopulations expressing memory-like gene modules: one is also present in blood (circulating precursors) and the other one in juxtatumor tissue (tissue-resident precursors). In tumors, these two precursor populations converge through a unique transitional state into terminally differentiated cells, often referred to as dysfunctional or exhausted. Differentiation is associated with TCR expansion, and transition from precursor to late-differentiated states correlates with intratumor T cell cycling. These results provide a coherent working model for TIL origin, ontogeny, and functional organization in primary NSCLC.

INTRODUCTION

Lung cancer is the leading cause of cancer-related death worldwide. Non-small cell lung cancer (NSCLC) represents 85% of lung cancer diagnoses (1), and tumor infiltration by lymphocytes is associated with a favorable survival prognosis (2) and a better clinical response to immune checkpoint blockade (ICB) (3). ICBs are thought to “re-program” CD8⁺ tumor-infiltrating lymphocytes (TILs) to produce antitumor responses (4, 5) by targeting inhibitory receptors such as programmed cell death protein 1 (PD-1), which are highly expressed by most TIL populations. How this reprogramming is achieved and which TIL subpopulations are targeted by ICBs are still open questions.

Most studies have distinguished early precursors and terminally differentiated CD8⁺ T cell populations (6, 7) in chronic viral infections and tumors. Early precursors present characteristics of memory cells, including memory/stem markers and regenerative capacity. They are characterized by high expression of the chemokine recep-

tor CXCR5, which is also expressed by B cells and follicular helper T cells (Tfh) (8, 9). These precursors are not fully committed and can therefore be “reprogrammed” by ICB (9). Terminally differentiated populations are clonally expanded and express higher levels of effector markers and immune checkpoints (ICPs)—including PD-1, T cell immunoglobulin and mucin domain-3 (TIM3), and CD39 (6, 9)—and share many characteristics with “exhausted” or “dysfunctional” CD8⁺ T cells. Dysfunctional TILs were initially described in chronic viral infection mouse models by poor effector function, expression of inhibitory receptors, low proliferation, and distinct transcriptional and epigenetic states compared with effector or memory T cells (10, 11). Several groups have recently analyzed T cell transcriptional programming in cancer, revealing a strong heterogeneity among TILs (12–17), similar to chronic viral infections, with distinct subpopulations of exhausted progenitors and terminally differentiated T cells. The idea that terminally differentiated T cells in cancer are dysfunctional, however, is still debated, especially in human tumors.

Here, we used a combination of single-cell RNA sequencing (scRNA-seq) and single-cell T cell receptor (TCR) sequencing (scTCR-seq) in tumors, normal tissues adjacent to the tumor (juxtatumor), and peripheral blood to delineate the processes of CD8⁺ T cell differentiation in patients with untreated, primary NSCLC. We show that precursor, memory-like CD8⁺ TILs are composed of two main populations: one is also present in the blood (circulating precursors) and the other is also present in juxtatumor tissue and bears markers of memory-resident T cells (resident precursors). Both precursor subtypes differentiate into a main population of terminal effectors through a similar “transitional” stage. Terminal effectors are not observed in blood or juxtatumor tissue, are more clonally expanded, and express signatures of exhaustion. A substantial proportion of transitional and terminal effectors also express cell cycle signatures and Ki67, suggesting that clonal expansion that occurs in situ is part of the terminal differentiation process.

¹PSL Research University, Institut Curie Research Center, INSERM U932, Paris, France. ²Department of Organismic and Evolutionary Biology, Harvard University, Cambridge, MA, USA. ³Institut Curie Genomics of Excellence (ICGex) Platform, Institut Curie Research Center, Paris, France. ⁴Centre d'Investigation Clinique Biothérapie, Institut Curie, Paris, France. ⁵Institut Curie, Institut du Thorax Curie Montsouris, Paris, France. ⁶Institut Montsouris, Surgery Department, Institut du Thorax Curie Montsouris, Paris, France. ⁷Paris 13 University, Sorbonne Paris Cité, Faculty of Medicine SMBH, Bobigny, France. ⁸PSL Research University, Laboratoire de physique statistique, CNRS, Sorbonne Université, Université Paris Diderot, Paris, France. ⁹PSL Research University, Laboratoire de physique théorique, CNRS, Sorbonne Université, Université Paris Diderot, and École normale supérieure, Paris, France. ¹⁰PSL Research University, Institut Curie Research Center, INSERM U830, Paris, France. ¹¹PSL Research University, Institut Curie Research Center, Department of Translational Research, Paris, France.

*These authors contributed equally to this work.

†These authors contributed equally to this work.

‡These authors contributed equally to this work.

§Corresponding author. Email: sebastian.amigorena@curie.fr (S.A.); joshua.waterfall@curie.fr (J.J.W.)

RESULTS

Transcriptional states of CD3⁺ TILs in NSCLC

We performed scRNA-seq on CD3⁺ T cells from 11 primary, untreated, and early-stage resected patients with NSCLC (Fig. 1A and table S1). For six of these patients, matched scTCR-seq information was also collected. Combined analysis of all patient samples identified a large source of variation associated with 3' versus 5'-oriented single-cell chemistries (fig. S1, A to C) that was resolved using computational methods (18). Rigorous assessment of intrasample heterogeneity, including TCR, showed that integration did not overcorrect the sample expression profiles. After removing contaminating cell types, we collected data on 28,936 cells over the 11 patients (Fig. 1B). Uniform manifold approximation and projection (UMAP) and unsupervised graph-based clustering partitioned cells into 21 clusters based on their transcriptome (Fig. 1, B and C). Differential gene expression analyses (fig. S1D and table S2) and analyses of canonical marker genes (Fig. 1D) revealed the identities of the major cell clusters. We used gene signatures (table S3) (17, 19–24) to reduce the impact of sparsity in the scRNA-seq values and assigned identities to different clusters, including naïve, memory, regulatory, helper, and effector T cells (Fig. 1E). Among these clusters, CD4⁺ regulatory T cells (T_{regs}) (CD4–IL--32–T_{regs}) and CD4⁺ memory (CD4–CD69–activated memory) are the most abundant, whereas the most abundant CD8⁺ subsets are CD8⁺–circulating precursors [CD8–Kruppel-like factor 2 (KLF2)] and transitional CD8⁺ [CD8–granzyme H (GZMH)] (Fig. 1C and fig. S1E). We identify 10 clusters of CD4⁺ cells [including C-C motif chemokine receptor 8 (CCR8)–T_{regs}, interleukin-32 (IL-32)–T_{regs}, GZMA effectors, SELL-naïve, CD69-activated memory, IL-7R–memory, myelin and lymphocyte protein (MAL)–T_{regs}, tumor necrosis factor receptor superfamily member 18 (TNFRSF18)–T_{fh}, sestrin 1 (SESN 1)–T_{fh}, and heat shock protein family H member 1 (HSPH1)–memory], 7 clusters of CD8⁺ cells [including FCGR3A effectors, KLF2–circulating precursors, GZMK–circulating precursors, XCL1–resident precursors, LAYN–terminally differentiated, GZMH–transitional, and SLC4A10–mucosal-associated invariant T cells (MAIT)], a cluster of $\gamma\delta$ T cells (TRDC), and 3 clusters of both CD4⁺ and CD8⁺ cells: one characterized by high expression of interferon (IFN)–related genes [CD4/8–IFN-stimulated gene 15 (ISG15)] and the other two characterized by strong expression of cycling genes (CD4/8–MCM5 and CD4/8–TOP2A). Analysis of ICP molecules expression showed that CD4–CCR8 cells express both inhibitory and stimulatory receptors, with particularly high levels of stimulatory molecules TNFRSF18 and TNFRSF4, whereas CD8–LAYN cells show higher expression of inhibitory molecules such as hepatitis A virus cellular receptor 2 (HAVCR2)/TIM3 and lymphocyte activating 3 (LAG3) (fig. S1F). All clusters are present in all patients, although at varying frequencies (fig. S1G). As CD8⁺ T cells are critical players during tumor rejection, we focus our analysis on this compartment.

Memory-like precursors and terminally differentiated CD8⁺ TILs

CD8⁺ T cells (10,243 cells after selection) segregate mainly along a horizontal axis in the UMAP, with cells expressing a stemness signature (Fig. 1E), central memory–related genes (including *IL7R*, *CXCR5*, and *TCF7*; Fig. 2A), and oxidative phosphorylation signatures (also related to T cell memory; Fig. 2A) at the left end of the axis. At the right end of the axis, cells express higher levels of effector-related genes (Fig. 1E), negative ICPs (Fig. 1E), including *HAVCR2*/*TIM3* and *ENTPD1* (Fig. 2A), *TOX* (a transcription factor involved in exhaustion, Fig. 2A), and a glycolysis signature (also associated with

effector function, Fig. 2A). Consistent with these results, exhausted precursor (GMZK/ZNF683) and terminally exhausted (LAYN) signatures from Guo *et al.* (13) are also highly expressed on the left and right ends of this axis, respectively. Comparison of the expression of signatures from a study on chronic viral infection in mice (19) in our data showed progenitor and terminal exhausted signatures with enhanced expression on the left and right ends of this axis, respectively (fig. S2, A and B). These results suggest that CD8⁺ T cell clusters on the left of the UMAP are “memory-like precursors” (clusters CD8–GZMK, CD8–KLF2, and CD8–XCL1) and that those on the right part of the UMAP (CD8–GZMH and CD8–LAYN) are more differentiated and most likely related to late exhausted/dysfunctional cells.

Memory-like precursors include two main subclusters, CD8–GZMK/CD8–KLF2 and CD8–XCL1, expressing high levels of the GZMK and ZNF683 signatures from Guo *et al.* (13), respectively (Fig. 2A). Memory-like precursors are enriched in signatures of negative regulation of cell proliferation, whereas terminally differentiated cells are enriched for lymphocyte activation-related genes and adhesion integrins (fig. S2B). We conclude that early-stage NSCLC TILs include two main populations of memory-like precursors (CD8–GZMK/CD8–KLF2 and CD8–XCL1) and two populations of late, differentiated cells (CD8–GZMH and CD8–LAYN) that may correspond to terminally exhausted TILs.

Two distinct circulating precursor subsets

Previous studies have associated precursor CD8⁺ TILs to a favorable prognosis and better response to ICB-based immunotherapies (17). To investigate the possible relevance of the different clusters defined here to clinical outcomes, we compared our dataset to a previous single-cell study from Sade-Feldman *et al.* (17) and applied signatures from melanoma patients responding (good response) versus not responding (bad response) to ICB. CD8–KLF2–circulating and CD8–XCL1–resident precursor clusters express higher levels of the good response signature (Fig. 2, B and C). In contrast, CD8–LAYN and CD8–GZMH late clusters, and a part of CD8–GZMK early clusters, express higher levels of the poor response signature (Fig. 2, B and C).

CD8–KLF2 and CD8–GZMK show similar global expression profiles but are discordant for the ICB prognostic signatures; thus, we performed differential analysis of gene expression between these two populations. Cells in the CD8–GZMK cluster overexpress genes related to T cell activation [human leukocyte antigen (HLA)–DR/DP/DQ], effector-related genes [killer cell lectin like receptor G1 (KLRG1), GZMB, GZMH, and GZMA, in addition to GZMK], and chemokines (*CXCR6* and *CCL5*) (Fig. 2, D and E). The CD8–KLF2 cluster overexpresses genes related to the control of CD8⁺ T cell differentiation, including *NR4A1/2/3* and *KLF2* (Fig. 2, D and E). These two closely related populations of CD8⁺ TILs are also present in other public datasets (13, 16, 17), including some generated on different technological platforms [switching mechanism at the end of the 5'-end of the RNA transcript sequencing (SMART-seq2)/massively parallel RNA single-cell sequencing (MARS-seq)] and in other tumor types, such as melanoma and breast carcinoma (fig. S2C). This supports the existence of subtle but important differences between these two populations and motivates further characterization of their relationship with respect to signaling and differentiation pathways.

Tissue-resident and transitional CD8⁺ populations

To better understand the different early and late TIL populations, and because one of the main driving genes among the three early

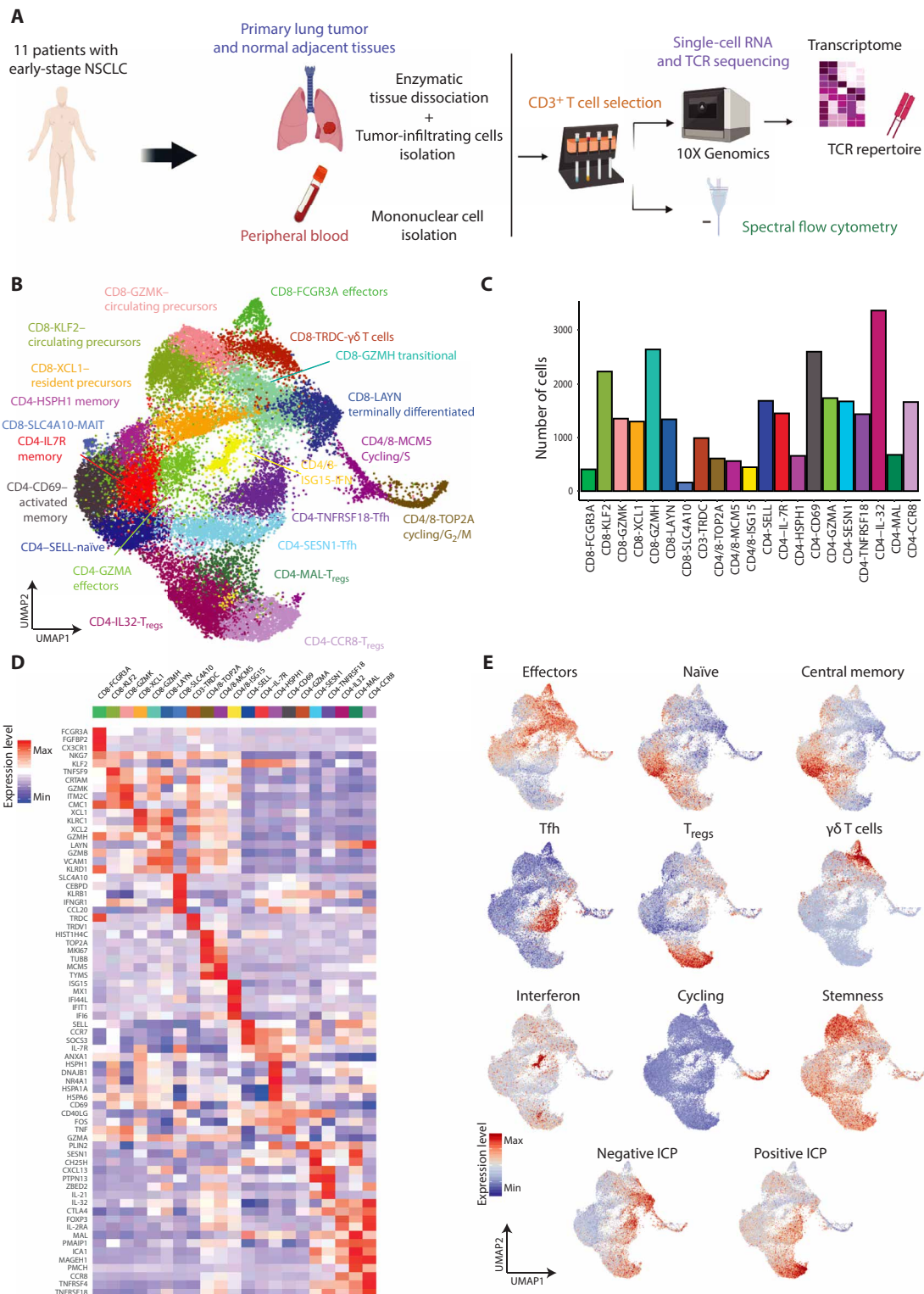


Fig. 1. Characterization of CD3⁺ TILs in NSCLC. (A) Graphical overview of the study design. scRNA- and TCR-seq were applied to tumor tissues, normal adjacent lung tissues, and blood samples derived from 11 primary, untreated patients with NSCLC. Spectral flow cytometry analysis was applied in an additional dataset of patients with the same clinical characteristics. (B) UMAP of 28,936 single CD3⁺ tumor-infiltrating T cells from 11 patients with NSCLC, showing the formation of 21 main clusters, including 7 for CD8⁺ cells, 11 for CD4⁺ cells, 1 for T cells highly expressing IFN-related genes, and 2 for cycling T cells. (C) Summary of the distribution of the number of cells contributing to each cluster. (D) Heatmap of expression values for the top genes with enriched expression in CD3⁺ T cells, found by *k*-nearest neighbors' subclustering. Expression values are zero-centered and scaled for each gene. (E) Projection of a selected set of marker genes and gene signatures, identifying T cell state. Each cell is colored on the basis of the normalized expression.

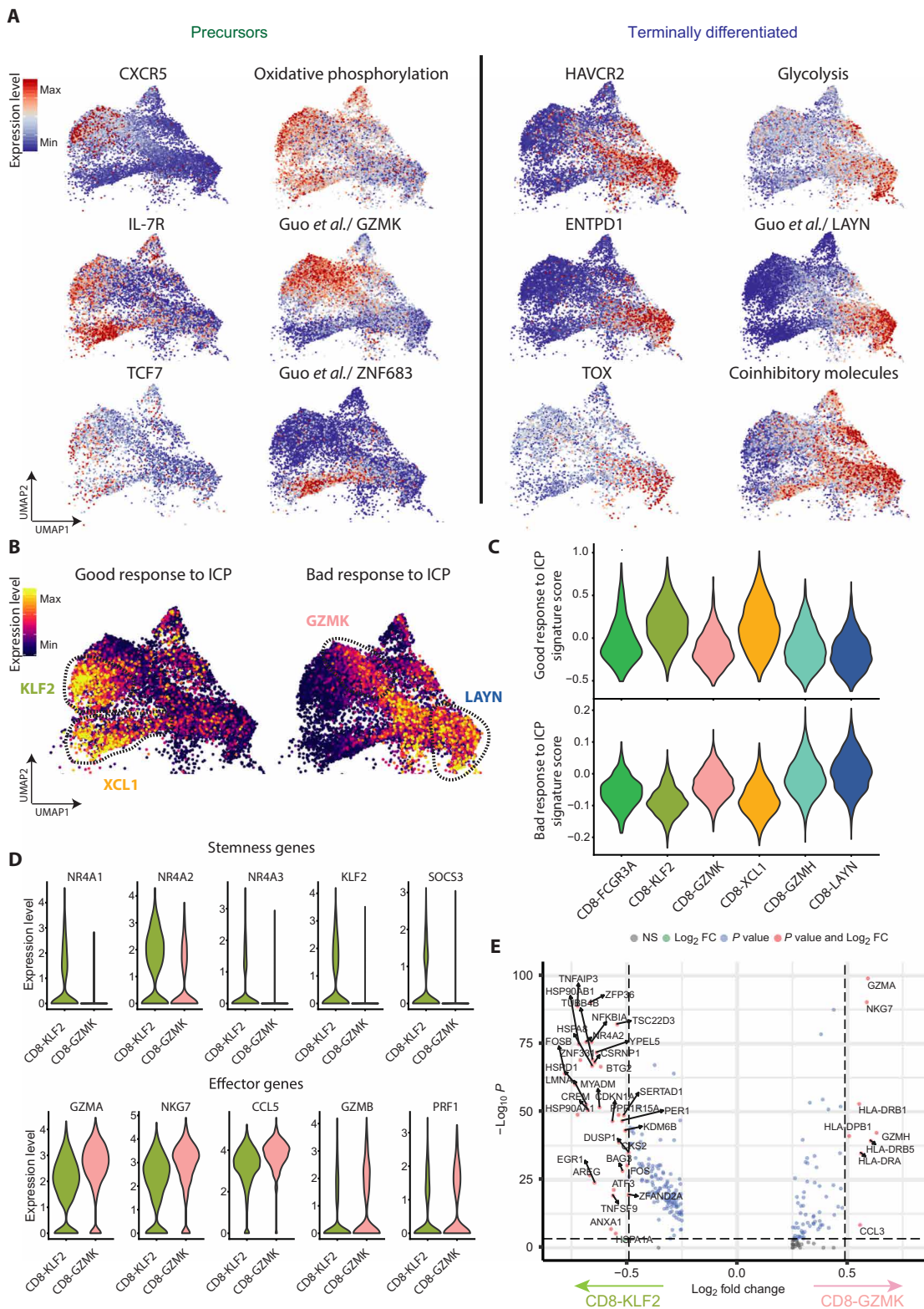


Fig. 2. Stem-like precursors and late dysfunctional CD8⁺ cells. (A) Expression of single marker genes and gene signatures for memory-like, precursors CD8⁺ cells (left) and terminally differentiated CD8⁺ cells (right), respectively. (B) UMAP projection of tumor-infiltrating CD8⁺ cells, with each cell colored based on the gene signature score of a published study in melanoma patients. (Left) The expression of genes associated with therapeutic response and improved outcome to anti-PD-1 treatment (good response). (Right) The expression of genes associated with bad response to anti-PD-1 treatment. (C) Violin plots of the distribution of the expression scores of the two gene signatures among the different CD8⁺ clusters. (D) Violin plots of differentially expressed genes between CD8-KLF2 and CD8-GZMK clusters. (E) Volcano plot of differentially expressed genes between CD8-KLF2 and CD8-GZMK clusters. Each red dot denotes an individual gene passing *P* value and fold difference thresholds.

clusters is ZNF683 [also known as Hobit, a transcription factor involved in the programming of tissue-resident memory CD8⁺ T cells (25)], we hypothesized that some clusters could correspond to tissue-resident cells and others to circulating cells. As shown in Fig. 3A and fig. S3A, single gene expression of ZNF683, as well as a core tissue residency gene signature, consisting of four main tissue-resident markers (ITGAE, ITGA1, CXCR6, and ZNF683), are all expressed at higher levels in late-differentiated CD8-GZMH/CD8-LAYN and in early CD8-XCL1 clusters, as compared with the CD8-GZMK/CD8-KLF2 clusters, which are characterized by enriched expression of KLRG1 (fig. S3A). These mRNA expression differences were validated at the protein level. Flow cytometry analysis of six additional patients with NSCLC showed that a higher proportion of CD103⁺ CD8⁺ TILs express markers related to T cell dysfunction, including PD-1, TIM3, and CD39, as compared with CD103⁻ TILs (Fig. 3, B to D and fig. S3B). The subset of CD103⁺ CD8⁺ TILs not expressing markers of T cell dysfunction, or expressing them at very low levels, likely corresponds to the CD8-XCL1-resident precursors that we identified in the scRNA-seq analysis, because transcript levels for inhibitory ICPs are low in this cluster (fig. S1F). A large fraction of CD103⁺ CD8⁺ TILs coexpresses T cell dysfunction markers and GZMB while showing lower expression of KLRG1, as compared with CD103⁻ CD8⁺ TILs (Fig. 3C). These results are consistent with recent studies (26–28) that found subsets of tissue-resident (CD103⁺) CD8⁺ TILs enriched in checkpoint receptors and display features of enhanced cytotoxicity and tumor reactivity, indicative of a therapeutic potential of this population.

Analysis of cluster membership as a function of clustering resolution showed that the split between CD8-XCL1 and CD8-KLF2/GZMK occurs early, indicating the importance and robustness of the differences (fig. S3C). On the basis of these results, we hypothesized that the two early, memory-like populations of CD8⁺ cells could correspond to tissue-resident cells (CD8-XCL1) and recent emigrants (most likely from blood, CD8-KLF2/CD8-GZMK; see below). We further speculated that the two types of precursors could both show converging differentiation into late-differentiated and dysfunctional/exhausted (CD8-GZMH/CD8-LAYN) subtypes.

To test this working model, we used two different unsupervised approaches to infer continuous transitions between clusters. Statistical analysis of connectivity in the *k*-nearest neighbor graph of cell-cell expression similarities [partition-based graph abstraction (PAGA)] (13–15, 29, 30) shows that the CD8-GZMH cluster represents a transitional state between early and late clusters (Fig. 3E). Because discretizing elements in a continuum of differentiation might not be optimal, we also used pseudotime alignment to resolve relationships between continuous populations. Monocle3 analysis revealed a converging differentiation process, consistent with the original UMAP representation and with PAGA analysis (Fig. 3F). As anticipated earlier, pseudotime reconstitution distinguishes separate resident and circulating precursor differentiation branches (Fig. 3F). Examples of differentially expressed genes between branches are shown in fig. S3D. With both tools, the CD8-GZMH cluster localized at the intersection between three branches (CD8-XCL1, CD8-KLF2/CD8-GZMK, and CD8-LAYN), suggesting that the CD8-GZMH cluster corresponds to a transitional population of cells undergoing differentiation from early, memory-like (CD8-XCL1 and CD8-KLF2/CD8-GZMK) to late, terminally differentiated (CD8-LAYN) clusters.

If the CD8-GZMH cluster represents a transitional state, then it should present lower clustering robustness, because cells from dif-

ferent clusters would enter this “state” and then differentiate into other states. We quantified robustness of clustering using the silhouette score (Fig. 3G and fig. S3E), which validates consistency by evaluating how close each cell inside a cluster is to its neighboring cells within the same cluster (high score), compared with its neighboring cells in other clusters (low score). As shown in Fig. 3G, the silhouette score is lower for cells in the CD8-GZMH cluster, as compared with cells in all other CD8⁺ clusters. Consistent with this analysis, label transfer, a method introduced for the integration of multiple single-cell datasets (18), of cells from the CD8-GZMH cluster shows even projection to the corresponding neighboring clusters, including CD8-GZMK (upper left part of the UMAP), CD8-XCL1 (lower left), and CD8-LAYN (to the right) (Fig. 3H and fig. S3F). Although our clustering algorithm identified one transitional GZMH cluster for statistical robustness, this is a heterogeneous population and subtle differences are likely to exist within this subpopulation. The likely dynamic nature of this transition process makes it challenging to track experimentally in human clinical samples. These results, as hypothesized earlier, are consistent with early precursor CD8⁺ populations (CD8-GZMK, CD8-KLF2, and CD8-XCL1) differentiating into terminally dysfunctional CD8-LAYN cells, via a transitional CD8-GZMH state.

Clonal sharing between clusters informs differentiation

To better understand the ontological relationships between the different TIL clusters, we sought to analyze their TCR repertoires. scTCR-seq for paired α and β chains from six patients was obtained, with matched 5' RNA profiling, for about 80% of the cells (table S4), including cells harboring unique or shared TCRs, indicative of clonal expansion. TCR clonotypes were called using the 10X pipeline when the analysis was restricted to one sample and a custom algorithm when the samples were distinct but autologous (31, 32). The clone size is defined as the total number of cellular barcodes associated with the same clonotype. Top clones cluster identities for each patient are shown in fig. S4A.

To investigate the extent of clonal expansion in different clusters, we first represented individual cells in colors according to the size of their TCR clones. As shown in Fig. 4 (A and B), larger clones are found within CD8⁺ T cell clusters as opposed to CD4⁺ and, more specifically, in late-differentiated (CD8-GZMH and CD8-LAYN) clusters, consistent with previous reports (13–15, 29, 30). This pattern was conserved across patients (Fig. 4B, bottom), as measured using either a published expansion index (12, 14) or by the mean number of cells per TCR clonotype. By visualizing all cells from individual TCR clones in the UMAP, we found that TCR clones are confined to specific clusters in most cases (examples in Fig. 4C).

To quantify whether there is a link between individual TCRs and specific clusters, we calculated the conditional probability that if a particular TCR is observed in one cluster, then it will also be observed in the same or other clusters. Unsupervised clustering of these probabilities is shown in Fig. 4D. The probability that the same TCR is found in cells from the same clusters is consistently higher than the probability to find the same TCR in cells from different clusters (dark blue diagonal). Nevertheless, there is an observable degree of TCR sharing across clusters and the probability to find the same TCRs in two different clusters is not zero. As illustrated by the light blue cases in Fig. 4D, “sharing” of TCRs between clusters occurs and is preferential between clusters with similar functional abilities. For example, the subclusters of CD4-T_{regs} share more TCRs among them than they share with CD4-T_{fh} or CD4-memory

Fig. 3. Tissue-resident and transitional CD8⁺ subsets. (A) UMAP projection of tumor-infiltrating CD8⁺ cells, with each cell colored on the basis of the relative normalized expression of a gene signature for tissue residency, consisting of the following genes: ITGAE, ITGA1, XCL1, and ZNF683.

(B) Flow cytometry plots of PD-1 and TIM3 expression in subsets of CD103⁺ CD8⁺ and CD103⁻ CD8⁺ cells. Frequency of CD103⁺ and CD103⁻ cells in eight different subsets of CD8⁺ TILs, defined by the expression of three inhibitory ICP molecules: PD-1, TIM3, and CD39. Data representative of six independent experiments/patients with NSCLC (**P ≤ 0.01, two-way ANOVA test). FSC-A, forward scatter-area.

(C) Representative tSNE analysis of tumor-infiltrating CD8⁺ cells with each cell colored based on the median fluorescence intensity of each of the markers: CD103, PD-1, TIM3, CD39, KLRG1, and GZMB. (D) Summary of the frequency of eight different CD8⁺ cell subsets inside CD103⁺ and CD103⁻ CD8⁺ cells. Data representative of six independent experiments/patients with NSCLC.

(E) Partition-based graph abstraction of CD8⁺ tumor-infiltrating cells, from 11 patients with NSCLC, connects circulating (GZMK and KLF2) and resident (XCL1) CD8⁺ precursors with terminally differentiated CD8⁺ (LAYN), through GZMH cluster, without any direct connection between effector CD8⁺ cluster (FCGR3A). (F) Trajectory of CD8⁺ tumor-infiltrating cells transition state, from 11 patients with NSCLC in a two-dimensional state-space determined by Monocle3. Each dot represents a single cell. Each color represents a different CD8⁺ cluster.

(G) Visualization of the silhouette coefficient score on the UMAP of the integrated CD8⁺ cells reference from 11 NSCLC tumor samples. Silhouette coefficient is calculated on the basis of the mean intracluster distance and the mean of the nearest cluster distance for each cell of each cluster. Each cell is colored on the basis of the score: 1 is the highest value, highlighted in purple and indicating robust clusters; -1 is the lower value, highlighted in gray and indicating less robust clusters; 0 is indicative of overlapping clusters.

(H) Label transfer of cell type labels from GZMH cluster onto the integrated CD8⁺ cells reference from 11 NSCLC tumor samples. Colored cells are cells from CD8-GZMH cluster and gray cells are coming from the other clusters.

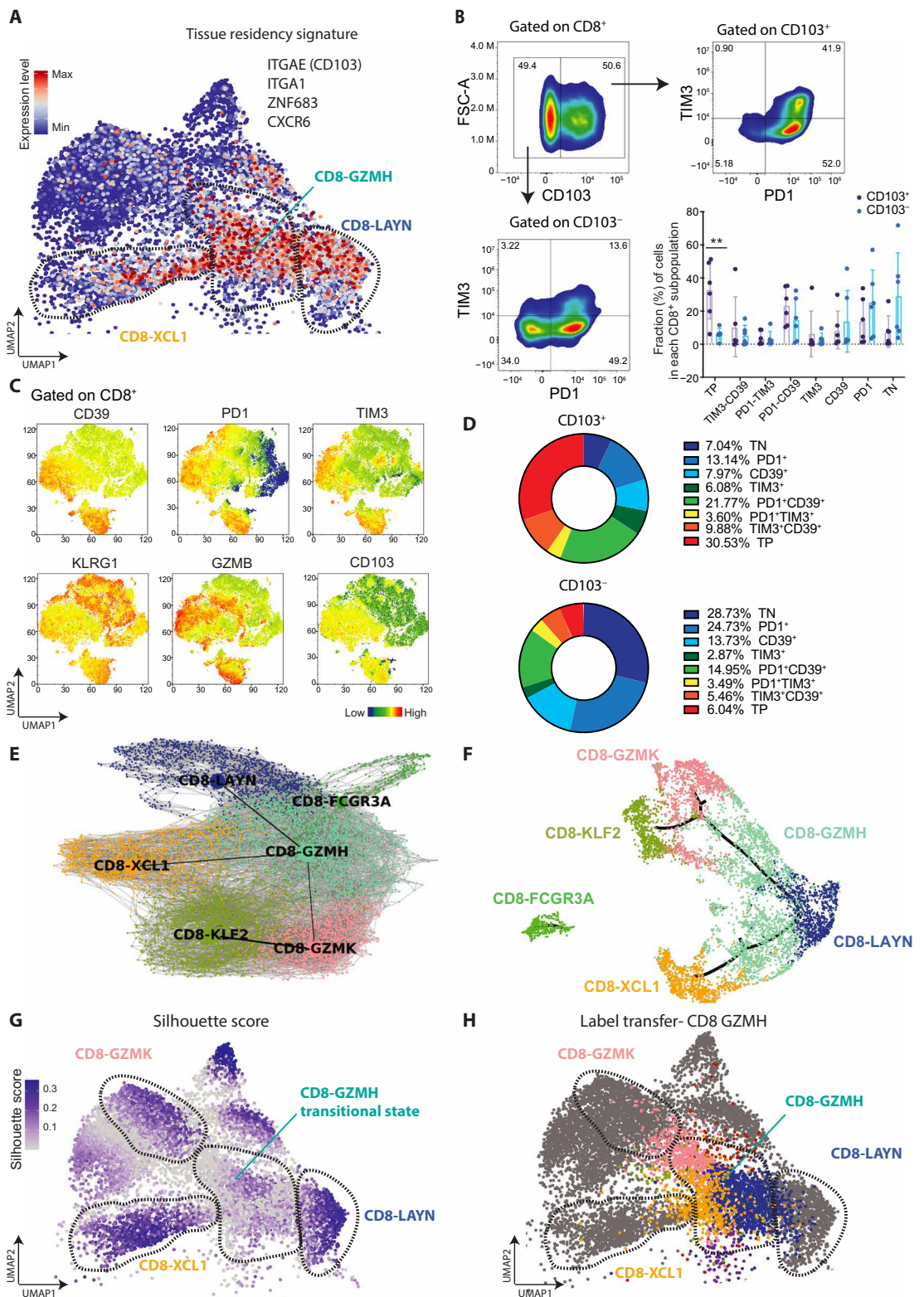
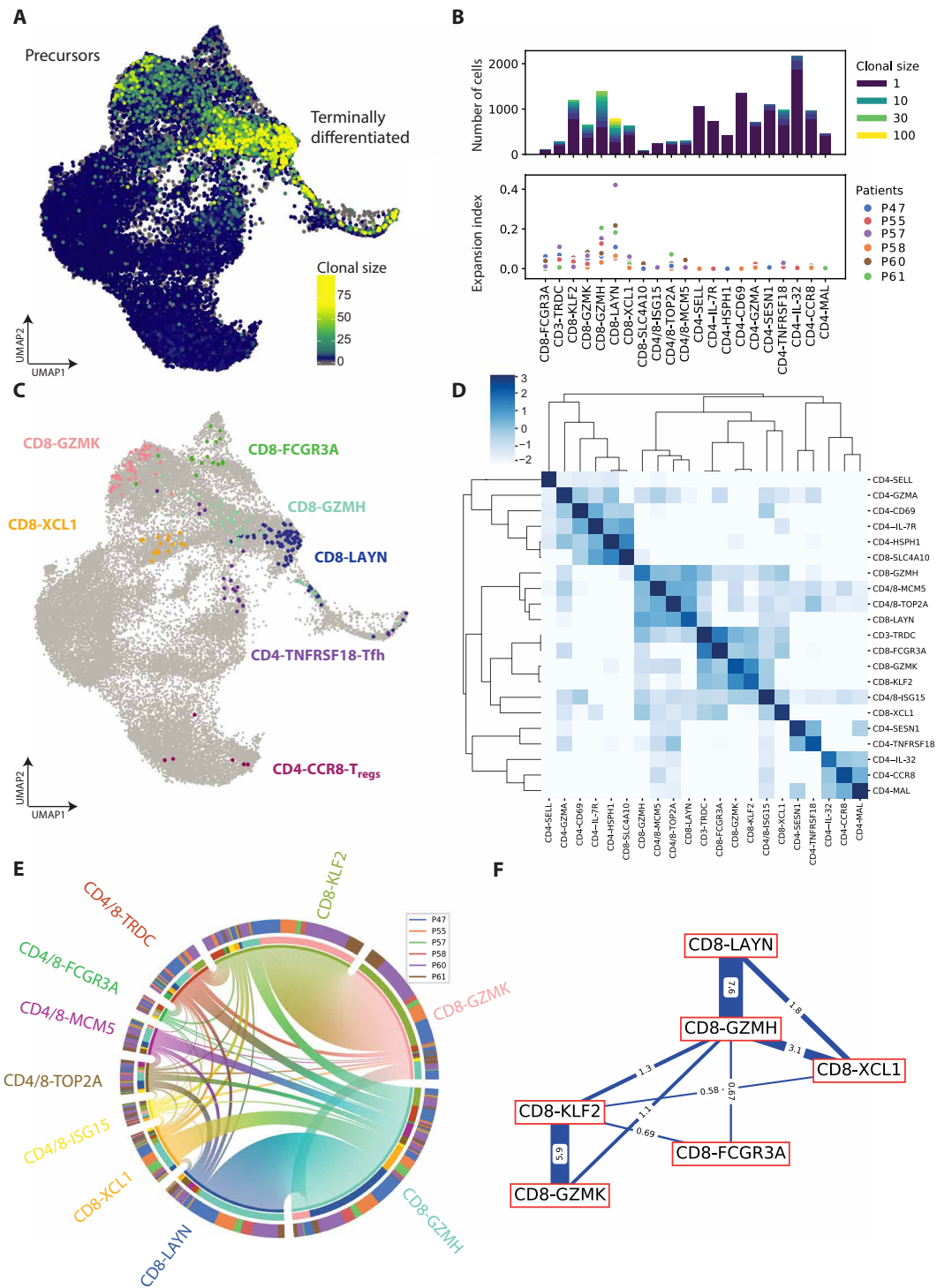


Fig. 4. Clonal expansion and TCR sharing in clusters. (A) Visualization of the clonal size on a UMAP embedding on the integrated 11 tumors reference. (B) Top: Quantification of clonal size per cluster identities. Bottom: Expansion index computed for each cluster and each patient. (C) Selected examples of cluster-specific clones from P60. (D) Normalized heatmap of clonal sharing probabilities (as defined in the subsection TCR analysis of the methods). (E) Circos plot of clonal sharing between clusters. Each line represents one shared clone with the most frequent sharing. (F) Scheme of sharing similarities between CD8 clusters as computed in (D).



T cell clusters. Among the CD8⁺ T cell clusters, increased sharing between circulating precursor memory-like clusters (CD8-GZMK and CD8-KLF2) and between differentiated clusters (CD8-LAYN and CD8-GZMH). The CD4/8-ISG15 (enriched for IFN-related genes) and the cycling clusters show increased sharing with early memory-like and late-differentiated clusters, respectively. We conclude that while high-intracluster TCR sharing highlights the relevance of our clustering strategy, intercluster TCR sharing can be used to infer transitions of cells between clusters: Higher TCR sharing between two clusters might indicate dynamic transitions of cells between the two transcriptional states. We conclude that intercluster TCR sharing can be used to infer a biologically relevant measure of proximity between clusters that can indicate either a dynamic transition between two transcriptional states or a static similarity not fully captured by transcriptome-based clustering methods.

To investigate potential transitions between clusters based on TCR sharing in more detail, we represented all the TCRs shared between two clusters in a “circos” representation (Fig. 4E), in which each line represents a single TCR clonotype. This representation illustrates that the two main circulating precursor memory-like clusters

(CD8-GZMK and CD8-KLF2) and the two main late-differentiated (CD8-GZMH and CD8-LAYN) clusters share numerous TCRs. We also computed the transition index using the single T-cell analysis by Rna-seq and Tcr TRACKing (STARTRAC) method (33), as the likeliness of a cluster to share clones (fig. S4B), and we see that CD8-LAYN and CD8-GZMH are the clusters that are most likely to have TCR sharing. The circos plot shows that GZMH displays higher clonal sharing with all the rest of the clusters (Fig. 4E and fig. S4C).

This result was reproducible between patients. The CD8-GZMH cluster shares over half of its shared TCRs with the CD8-LAYN cluster, whereas the other half is shared with other CD8⁺ T cell clusters (fig. S4C). Supervised representation of the computed probabilities of shared TCRs among clusters (Fig. 4F) shows that the CD8-GZMH cluster could represent a central hub, sharing TCRs with both early, memory-like, and late-differentiated clusters. The high levels of TCR sharing between clusters were confirmed by analysis of the number of T cells from each cluster for shared clones. As shown in fig. S4D, “equilibrated” sharing between clusters, when the same TCR is present in three or more cells from each cluster, is only seen between CD8-GZMH/CD8-LAYN and CD8-GZMK/CD8-KLF2 and, to a lower extent, between XCL1/GZMH. Equilibrated sharing suggests active transitions between clusters. As proposed below, TCR-sharing analysis is consistent with the GZMH cluster representing a transitional state between the two main populations of memory-like precursors (CD8-KLF2/CD8-GZMK and CD8-XCL1) and the late-differentiated cells present in the CD8-LAYN cluster.

Terminally differentiated, not memory-like, CD8⁺ T cells are in cell cycle

The question of the cycling activity of early memory-like versus late terminally differentiated TILs is still a matter of debate (34). As T cells require TCR signaling to enter the cell cycle, clones identified to be actively cycling intratumorally strongly suggest a local intratumor source of antigen. Cell cycle-related genes are expressed at high levels, and thus, cycling cells cluster independently in scRNA-seq analyses. These clusters, however, may include cells that also bear underlying signatures from other clusters, which are in some way masked by highly expressed cell cycle genes. We took two independent approaches to investigate whether the cells in the cycling cluster are related to other clusters.

We focused first on the transcriptomic dataset, and clustering of the infiltrating T cells in 11 patients with NSCLC shows two different cycling populations, one in G₂-M phase (CD4/8-TOP2A) and the other one in S phase (CD4/8-MCM5) (fig. S5A). To better characterize these clusters, we used label transfer to interrogate the “second best” cluster to each cycling cell. The IFN-related cluster (CD4/8 ISG15) also includes CD4⁺ and CD8⁺ T cells, and ISGs are also highly expressed and can drive independent clustering of cells related to other clusters, so we included this cluster in the same label transfer analysis. Label transfer of CD8⁺ cells from the CD4/8 ISG15 cluster shows that they recluster mainly to CD8-GZMK and CD8-GZMH clusters (Fig. 5, A and B). Label transfer of CD8⁺ T cells from the cycling clusters results in almost exclusive reclustering to late-differentiated effector clusters CD8-GZMH and CD8-LAYN (Fig. 5, A and B). Almost no cells from the cycling clusters are reattributed to progenitor CD8⁺ T cell populations, suggesting that cycling cells are transcriptionally closer to late-differentiated T cells.

We validated these results using flow cytometry analysis in freshly isolated TILs from 10 additional patients with NSCLC. As shown in Fig. 5 (C and D), CD8⁺ cells coexpressing PD-1, TIM3, and CD39 [triple-positive (TP)] are also Ki67⁺. CD8⁺ T cells negative for the three inhibitory ICP markers or expressing only PD-1 show very low Ki67 labeling (Fig. 5, C and D). t-distributed stochastic neighbor embedding (tSNE) visualization of cytometry data shows that a tissue-resident (CD103⁺) subset of these proliferative TP CD8⁺ cells also expresses PD-L1, suggesting that this subpopulation may play an important role in ICP response (fig. S5B).

The LAYN signature has previously been associated with exhausted/dysfunctional CD8⁺ T cells (13, 33, 35, 36). Among cycling cells, the ones transcriptionally related to the CD8-LAYN cluster by label transfer also express higher levels of DNA damage repair genes (fig. S5C). These cells express higher levels of gene signatures for DNA damage repair and stress (Fig. 5E) and of the terminally differentiated LAYN signature (fig. S5D) (13), as compared with cycling cells reattributed to the CD8-GZMH cluster. Analysis of the dataset of Guo *et al.* (13) for the cycling signature shows that the LAYN and the cycling populations overlap (fig. S5E), suggesting that late differentiating cells, and not early progenitors, are the main cycling T cells in NSCLC TILs.

We reasoned that if late differentiating cells cycle, then clonally amplified TCRs in these clusters should also be found in cycling T cells. Circos representation shows that the TCRs expressed in cycling cells are found preferentially in cells from late-differentiated effector CD8-GZMH and CD8-LAYN clusters (Fig. 5F). As shown in fig. S5F, preferential TCR sharing of cycling cells with late-differentiated clusters is not due to the larger size of these late clones. CD8-GZMK/CD8-KLF2 clones of more than 20 cells still share very few TCRs with the cycling cluster, as compared with CD8-GZMH/CD8-LAYN clones of similar sizes. Increased sharing can also be visualized in the sharing probability graph shown in Fig. 4D. Therefore, cycling cells share TCRs preferentially with late effectors, as compared with early memory-like precursors.

The results presented thus far are consistent with the possibility that transition between CD8-GZMH and LAYN clusters occurs while cells divide. To test this hypothesis, we measured the frequency of cycling cells among clones shared between the different clusters. As shown in Fig. 5G, most of the shared clones that include GZMH and LAYN cells also have TCRs in the cycling clusters (more red central dots in the left panel as compared with the right panel, Fig. 5G). Figure S5G uses a similar representation to show that the TCR clones found in the GZMH, LAYN, and cycling clusters include TCRs also present in the XCL1 cluster more frequently than TCRs also present in the GZMK cluster.

These results suggest that the preferential pathway toward terminal differentiation in tumors originates in the CD8-XCL1 cluster and transitions through CD8-GZMH to CD8-LAYN while cell divide and clonally expand. These data further support a model in which many expanded CD8⁺ TIL clones are actively cycling within the tumor, likely recognizing local sources of antigen in the tumor microenvironment. Furthermore, among CD8 subpopulations, the CD8-GZMH and CD8-LAYN clusters are potentially the most enriched for such local antigen specificity, as they show the strongest evidence for active cycling. It should be noted that this does not mean that tumor-specific TCRs are completely restricted to the GZMH and LAYN clusters nor does it guarantee that all local antigens are tumor specific. This model is consistent with these cells being chronically stimulated and with recent results in chronic human inflammation (37).

Resident versus circulating origin and tissue distribution of TILs

We analyzed scRNA- and TCR-seq in TILs from blood and juxtatumor tissue to further investigate the tissue versus blood origins of the different TIL populations described thus far. We obtained blood samples from four of the previously described patients and juxtatumor tissue samples from two patients. scRNA- and scTCR-seq in all

four patients resulted in 54,247 validated cells, with ~80% RNA- and TCR-coupled data. After removing contaminating cells and integrating the three different tissues, we used the clusters that have been identified before in the 11 different NSCLC tumor samples as a reference (as shown in Fig. 1B).

We quantified the proportions of the different populations in the different tissues by integrating cells from the three different tissues in these patients and used label transfer to map the populations from blood and juxtatumor to the tumor reference (Fig. 6, A to C). This allowed us to focus on conserved patterns between our tumor reference and the other tissues and minimize oversmoothing induced by integrating data from different tissues (fig. S6A). The CD4-SELL cluster (naïve T cells) contains mostly cells from blood, whereas the CD8-LAYN cluster (terminally differentiated) contains almost exclusively cells from tumors (Fig. 6, A to C, and fig. S6B). This result is consistent with flow cytometry analysis in four additional patients with NSCLC, showing that TIM3⁺ CD39⁺ CD8⁺ cells are enriched in the tumor samples, as compared with blood samples, which contain mainly single-positive PD-1⁺ or TN CD8⁺ cells (fig. S6C).

The CD8-XCL1 cluster (resident precursors) contains mostly cells from tumor and juxtatumor tissue (not from blood), indicating that it is a tissue-specific population, whereas cells in the CD8-GZMK and CD8-KLF2 clusters are also present in blood. These results are consistent with the proposed dual origin of memory-like progenitors: CD8-KLF2/CD8-GZMK cells originate from blood and could represent circulating precursors, whereas CD8-XCL1 cells absent from blood, but in juxtatumor tissue, may represent tissue-resident precursors (Fig. 6, B and C). The most abundant CD8⁺ T cell cluster in blood is CD8-FCGR3A, which are also present in juxtatumor samples but are rare in tumors (Fig. 6, B and C). Consistent with our model, CD8-GZMH (transitional) and CD8-LAYN (terminal) clusters are phenotypes acquired in tissue (Fig. 6B). The absence of CD8-LAYN cells in blood and juxtatumor is also consistent with CD8-GZMH cells becoming CD8-LAYN only in the tumor microenvironment.

We used scTCR information to further test this model. Most TCR expanded clones in the three tissues are present within CD8⁺ T cell populations (Fig. 6D). The clusters with the most expansion, however, are distinct in each tissue: the CD8-LAYN cluster in tumors (as shown before), the CD8-XCL1 cluster in juxtatumor, and the CD8-FCGR3A (together with the CD8-GZMK/CD8-KLF2 clusters) in blood (Fig. 6D). Analysis of shared TCR clonotypes present in tumor and blood (Fig. 6E) shows extensive TCR sharing between CD8-GZMK and CD8-KLF2 clusters in the two locations. Many expanded CD8-GZMK TCRs in blood are expressed in CD8-KLF2 cells in tumor, suggesting that CD8-KLF2 TILs may be derived from CD8-GZMK blood cells.

To further investigate possible ontological associations between clusters in blood and tumor, we analyzed the top 20 TCR clones per cluster in the blood (Fig. 6F, top) or in the tumor (Fig. 6F, bottom) for their transcriptional programming and TCR numbers in the other tissue (blood for tumor and tumor for blood). The top 20 TCR clonotypes from late-differentiated tumor clusters (CD8-GZMH and CD8-LAYN) were not observed in the blood, consistent with these clones expanding intratumorally. Among the top 20 CD8-XCL1 TCR clonotypes from the tumor, only one was also found in blood, where it has CD8-GZMK transcriptional programming. This result is consistent with most CD8-XCL1 clones not coming from blood

but from tissue-resident origin. Among the top 20 tumor clonotypes in the CD8-KLF2 and CD8-GZMK clusters, all are found at substantial frequencies in blood. However, whereas top tumor CD8-GZMK clonotypes are also mapped to CD8-GZMK cells in blood, top tumor CD8-KLF2 clonotypes are also found in CD8-GZMK clustered cells in blood (as suggested by the circos analysis; Fig. 6E). Analysis of the top 20 clonotypes per cluster from the blood yields consistent results. First, most expanded clones in blood are in the CD8-GZMK cluster, and most of these clones are also found in the tumor, where they display transcriptomic reprogramming corresponding to both CD8-KLF2 and CD8-GZMH clusters, mainly. This result suggests that TCR expanded CD8-GZMK blood CD8⁺ T cells are the main blood precursors for tumor infiltration. This also suggests that after infiltration, blood TCR expanded CD8-GZMK precursors are reprogrammed to other phenotypes including CD8-KLF2 and CD8-GZMH.

DISCUSSION

We used scRNA- and scTCR-seq to analyze CD8⁺ TILs, juxtatumor tissue, and blood in early-stage resected patients with NSCLC. On the basis of integration of transcriptomic programming with TCR in the three tissues, we propose an integrative working model for TIL origin, differentiation, and functional organization in primary NSCLC (Fig. 6G). Although we used multiple complementary approaches to derive this model, it should be noted that they are based on computational inference from static molecular snapshots and that directly assessing such inherently dynamic processes requires longitudinal sampling of individual patients (29).

The most abundant and clonally expanded population of CD8⁺ T cell effectors in blood (CD8-FCGR3A) is rare in tumors as are the clonal TCRs they express, indicating that these cells either do not infiltrate tumors effectively or die rapidly upon infiltration. If the cells entered tumors and changed phenotypes, then their TCRs would still be present in other clusters. This population also specifically expresses CX3CR1 (Fig. 1D), which has been used to identify a population of TILs with some markers of effector activity (13–15, 33). The position of this population with respect to TIL differentiation pathways has been unclear, with some studies describing it as an intermediate state in a linear pathway to exhaustion (15), others as an alternative end state to exhaustion in a branched pathway (13, 33), and yet others as an independent population not linked to intratumoral T cell differentiation (14). Our results, including trajectory analyses, TCR sharing, and cross-tissue comparisons, are most consistent with the final model. CD8-GZMK cells, in contrast, are abundant and clonally expanded in both blood and in tumors and share similar TCRs, suggesting that they represent the main blood precursor for TILs. A large proportion of the TCRs present in the CD8-GZMK cluster are also present in tumors in a second cluster of memory-like cells, CD8-KLF2, suggesting that these two populations are in dynamic equilibrium. Although trajectory reconstitution suggests that these two populations can differentiate into transitional CD8-GZMH cells, TCR sharing between the two is relatively low as compared with the sharing between CD8-XCL1 and CD8-GZMH. This result suggests that the transition between CD8-GZMK/CD8-KLF2 and CD8-GZMH is slow or inefficient. The other main population of early, memory-like, CD8⁺ T cells is in the CD8-XCL1 cluster. These cells express tissue-resident signatures and markers and are absent from blood, suggesting their tissue-resident

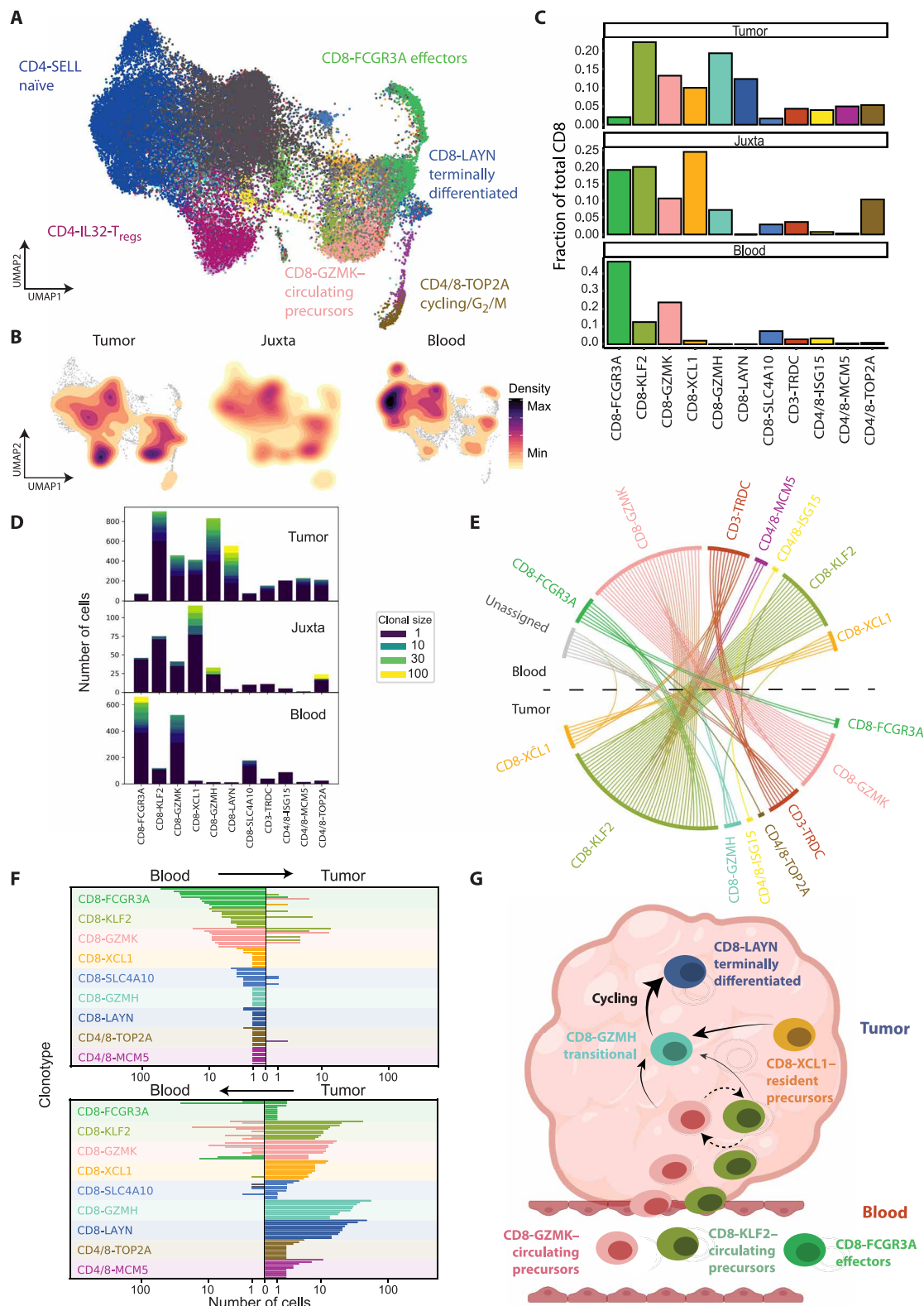


Fig. 6. Tissue-specific features—integrative model. (A) UMAP representation of the integrated cells from 17 samples from tumor, juxtatumor, and blood. (B) UMAP representation of cell densities split by the three tissues. (C) Scaled proportions of cells per clusters across the three tissues. (D) Quantification of clonal expansion for each cluster across the three tissues. (E) Circos plots of clonal sharing between tumor and blood cells. Each line represents one shared clone with the most frequent sharing. (F) Top 10 shared clones of blood (top) and tumor (bottom) being shared with tumor and blood, respectively, for each CD8 cluster. (G) Summary scheme of CD8 circulation and differentiation in NSCLC. Graph created using BioRender software (BioRender.com).

origin. These cells share numerous expanded TCRs with CD8-GZMH cells, suggesting that they represent the main source of GZMH transitional cells. Previous studies have described TILs with markers shared by our CD8-XCL1 cluster not as a precursor population but rather as either an intermediate differentiation state (13) or as a final resident memory state in a branched differentiation pathway (33). One potential reason for these differences is that these previous studies used plate-based approaches for scRNA-seq, which generally profiles fewer cells per sample than the droplet microfluidics technology we used. This difference gives our dataset more power in terms of TCR repertoire analysis, both for quantifying expansion and intercluster sharing.

The effector-like, late CD8⁺ TILs are divided into two clusters: CD8-GZMH and CD8-LAYN. Cells in the CD8-GZMH cluster show limited robustness in clustering and share numerous clonal TCRs with all other CD8⁺ T cell clusters, indicating that early memory like cells (circulating or tissue resident) transit through this stage before entering late terminally differentiated, most likely dysfunctional states (CD8-LAYN). Determining whether consistent, subtle differences exist between cells within the GZMH cluster, for instance, depends on whether they were derived from tissue-resident or circulating precursors and is unclear with our current dataset. Cells in the CD8-LAYN cluster belong to the larger TCR clones, most of which are shared with the CD8-GZMH cluster. Consistent with the idea that transition between these two late clusters requires cell divisions, a large proportion (~40%) of these late-stage cells shows strong cell cycle signatures and are labeled by Ki67 antibodies. Intratumor expansion of these cells, together with expression of T cell activation markers, suggests that the cells recognize antigens intratumorally, whether tumor specific or not. Tissue-resident CD8-XCL1 cluster cells share most TCRs with the CD8-GZMH/CD8-LAYN clusters, so we hypothesize that tumor antigen-specific T cells are derived mostly from tissue-resident memory populations (rather than from clones recently stimulated by antigen in the tumor-draining lymph nodes). The highly expanded TCRs present in blood (mainly in CD8-GZMK cluster cells) remain in early/memory-like clusters and are rare in late clusters, suggesting inefficient intratumor progression from blood precursors to terminally differentiated cells.

We did not investigate whether cells in the CD8-LAYN cluster are active effectors or dysfunctional/terminally exhausted in this study. Several recent papers provide partial evidence in each direction, depending on the types of tumors and markers used (14, 19, 28, 36–38). Here, we show that the CD8-LAYN cluster expresses high levels of a “bad response” signature to ICP in melanoma. We also found that cycling cells with LAYN-signature expression also highly express endoplasmic reticulum (ER) stress and DNA repair signatures, as compared with both noncycling cells from the same cluster and to cycling cells from the CD8-GZMH cluster (Fig. 5E). These results are consistent with cycling LAYN cells being exhausted/dysfunctional, rather than actively involved in tumor rejection.

In contrast to CD8-LAYN cells, very few memory-like CD8⁺ T cells were found to bear cell cycle signatures. In mice, several studies show that progenitor, memory-like TILs cycle (36–38), but the findings with human cells are more unclear. Recent papers suggest that TILs in early dysfunctional state in melanoma cycle (14), whereas other studies in NSCLC are consistent with our results, showing that more terminally differentiated cells that highly express inhibitory ICP molecules cycle more than early progenitors (12). The working model for TIL infiltration and differentiation

proposed here would predict that TCR expansion in the CD8-LAYN cluster, most likely exhausted or dysfunctional T cells, will not indicate a good prognosis for clinical responses to ICP blockers. Clinical responses to ICP blockade should be distinguished from the ability of ex vivo expanded TILs to recognize autologous tumor. Our results suggest that the CD8-GZMH and CD8-LAYN clusters are likely to be enriched for tumor-specific TCRs, consistent with reports that these populations show the highest proportion of tumor specificity by such experiments (12, 14). Among early, memory-like, and potentially reprogrammable CD8 clusters, our results suggest that TCR expansion in CD8-XCL1, rather than CD8-KLF2/CD8-GZMK, cluster cells could suggest a good prognosis for responses to ICB. Future scRNA-seq studies in patients with NSCLC responding or not to ICB will test this hypothesis.

MATERIALS AND METHODS

Study design

The overall objective of this study was to characterize the diversity and ontogeny of CD8⁺ T cells infiltrating untreated lung tumors. This was accomplished by performing scRNA-seq and TCR-seq and flow cytometry analysis on T cells isolated from tumor, juxtatumor, and blood samples from patients undergoing surgical resection for early-stage lung cancer. All samples were collected from the Institute Mutualiste Montsouris, under a dedicated protocol for lung cancer specimens approved by the French Ethics and Informatics Commission (EUdract 2017-A03081-52). All patients in this study provided written informed consent for sample collection and data analysis. Cohort size was selected to assess interpatient variability in subpopulation levels, and the number of cells per sample was selected to robustly estimate the frequency of subpopulations of at least 10% abundance.

Human specimens

Twenty-one patients, who were pathologically diagnosed with NSCLC, were enrolled in this study. Eleven were profiled by single-cell sequencing technologies, including 10 patients with adenocarcinoma and 1 patient with squamous cell carcinoma. The remaining 10 patients were profiled by flow cytometry analysis. All patients were untreated, with early-stage disease. Tumor tissue samples were obtained from all 21 resected patients with NSCLC. For four of the patients profiled by scRNA-seq, paired peripheral blood was collected and analyzed. Among those four, two patients had matched adjacent normal lung tissue collected and analyzed. For five of the patients profiled by flow cytometry analysis, paired peripheral blood was collected and analyzed. Among those five, two patients had matched adjacent normal lung tissue collected and analyzed. All samples were collected from the Institute Mutualiste Montsouris, under a dedicated protocol for lung cancer specimens approved by the French Ethics and Informatics Commission (EUdract 2017-A03081-52). All patients in this study provided written informed consent for sample collection and data analysis. All clinical information is summarized in table S1.

Tumor tissue and adjacent normal lung tissue were obtained from surgical specimens after macroscopic examination of the tissue by a pathologist. Tissue samples were stored in CO₂-independent medium (Invitrogen) with 10% human serum and transferred within 1 hour after surgery to the research institute. For each specimen, a fragment was formalin-fixed and paraffin-embedded for histology and immunohistochemistry.

Tissue dissociation

Tumor and adjacent normal lung tissue samples were gently cut in about 1-mm³ pieces. Tissues were digested enzymatically by a 20- to 40-min incubation, based on the size of the tissue, at 37°C under agitation, in CO₂-independent medium (Invitrogen) with collagenase I (2 mg/ml; Sigma-Aldrich), hyaluronidase (2 mg/ml; Sigma-Aldrich), and deoxyribonuclease (25 µg/ml; Sigma-Aldrich).

The tissue pieces were gently dissociated with a 20-ml syringe plunger on a 40-µm cell strainer (BD) in 1× phosphate-buffered saline (PBS) (Invitrogen) with 1% fetal bovine serum (FBS) and 2 mM EDTA (Gibco) until uniform cell suspensions were obtained. The suspended cells were subsequently centrifuged for 10 min at 400g.

TILs isolation

TILs were isolated using Ficoll-Paque PLUS solution (Sigma-Aldrich). After tissue digestion, cells were resuspended in CO₂-independent medium and layered onto Ficoll-Paque PLUS solution. Cells were centrifuged for 20 min at room temperature at 400 relative centrifugal force (RCF) without breaking. After centrifugation, TILs were carefully transferred to a new tube and washed with 1× PBS with 1% FBS and 2 mM EDTA (Gibco).

Peripheral blood mononuclear cell isolation

Peripheral blood mononuclear cells (PBMCs) were isolated using Ficoll-Paque PLUS solution (Sigma-Aldrich). Fresh peripheral blood was collected before surgery in EDTA anticoagulant tubes. Eight milliliters of fresh peripheral blood was resuspended in 1× PBS (Invitrogen) with 1% FBS and 2 mM EDTA (Gibco) and layered onto Ficoll-Paque PLUS solution. Cells were then centrifuged for 20 min at room temperature at 2000 rpm without breaks. After centrifugation, TILs were transferred to a new tube and washed with 1× PBS with 1% FBS and 2 mM EDTA (Gibco).

CD3⁺ T cell isolation and purification

CD3⁺ T cells from all samples were enriched using magnetic positive selection; CD3 microbeads and MACS separation (Miltenyi Biotec). Subsequently, dead cells and debris were removed, following the manufacturer's instructions (dead cell removal kit and debris removal kit, Miltenyi Biotec) resulting in ~80% of purity and CD3⁺ T cells were resuspended in 1× PBS with 0.04% bovine serum albumin. Cell numbers and viability were measured using a Countess II Automated Cell Counter (Thermo Fisher Scientific) as well as classical hemocytometer and trypan blue.

scRNA-seq and TCR profiling

Single-cell suspensions were loaded onto a Chromium Single Cell Chip (10X Genomics) according to the manufacturer's instructions for coencapsulation with barcoded gel beads at a target capture rate of 5000 to 10,000 individual cells per sample, based on the initial number of cells per sample. Referring to the blood samples, the target capture rate was 10,000 individual cells, whereas for tumor tissue and normal adjacent lung tissue samples, it was diverse between 5000 and 10,000 individual cells, due to the different cell number per tissue. For patients P34, P35, P42, P43, and P46, captured mRNA was barcoded during cDNA synthesis and converted into pooled scRNA-seq libraries for Illumina sequencing using the Chromium Single Cell 3' Solution (10X Genomics) according to the manufacturer's instructions. For patients P47, P55, P57, P58, P60, and P61, RNA and TCR libraries were synthesized by following the

Chromium Single Cell 5' V(D)J Enrichment Kit, Human T Cell (10X Genomics).

Flow cytometry

Flow cytometry analysis was performed in a dataset of 10 additional untreated patients with NSCLC, in early disease stage. For the isolation of lymphocytes from tumor tissue and normal adjacent lung tissues and of PBMCs, the same steps predescribed above were followed. For negative selection of CD3⁺ T cells, we used the Pan T cell Isolation Kit (Miltenyi Biotec) that leads to about 80% purity. Gating strategy: Cells were gated avoiding doublets and debris. Dead cells were excluded by surface staining with a LIVE/DEAD fixable Zombie NIR viability kit (1:1000; BioLegend, lot number B262784) for all experiments. CD8⁺ T cells were stained with a combination of surface markers. Exclusive antibody list is included in Supplementary Materials and Methods. Gating was applied by using monocolors and fluorescence minus one (FMO) controls. Data analysis was performed using FlowJo v.10.6.1. Intracellular staining was performed using the eBioscience intracellular fixation and permeabilization buffer set (Thermo Fisher Scientific) according to the manufacturer's guidelines. All samples were analyzed using a Cytex Aurora spectral flow cytometer.

Software versions

Data were collected using Cell Ranger software (10X Genomics) v2.0.1/v3.0.2 and analyzed using R v.3.5.1, and the following packages and versions in R for analysis: Seurat v3.1.1, ENHANCE v1.0.0, DropletUtils v1.8, clustree v0.4.1, and cluster v2.1.0 two-dimensional gene expression maps, were generated using coordinates from the UMAP algorithm using the R package uwot v0.1.3 implementation. Figures were produced using the following packages and versions in R: RColorBrewer v1.1-2, pheatmap v1.0.12, ggplot v3.2.0, and ggsignif v0.6.0.

scRNA/TCR-seq data processing

Single-cell expression was analyzed using the Cell Ranger Single Cell Software Suite (v2.0.1 and v3.0.2 for P58, P60, and P61, 10X Genomics) to perform quality control, sample demultiplexing, barcode processing, and single-cell 3' and 5' gene counting. Sequencing reads were aligned to the GRCh38 human reference genome (Ensembl 84).

Pathway enrichment

Pathways enrichment tests were performed using Metascape (using <https://metascape.org/> as of February 2020) (39) with default parameters using differentially expressed genes between early precursors (CD8-KLF2, CD8-GZMK, and CD8-XCL1) and terminally differentiated CD8⁺ T cells (CD8-GZMH and CD8-LAYN). Gene sets from MSigDB (v.7.0) were downloaded in GMT format from www.gsea-msigdb.org/gsea/msigdb/collections.jsp. These gene sets were used as modules for the AddModuleScore function in Seurat.

Data reprocessing

Data from Guo *et al.* (13) were downloaded from GSE99254. Data from Sade-Feldman *et al.* (17) were downloaded from GSE120575. Data from Azizi *et al.* (16) were downloaded from GSE114727 and reprocessed using Seurat v3 pipeline using the same preprocessing as described previously.

Trajectory analysis

To compute pseudotime alignment of our transcriptomes, we first used Monocle3 (v2.99.1) using the first 30 PCs of the integrated

matrix to preform preprocessing and UMAP reduction. DDRTree algorithm was then used to reconstruct the tree embedding. PAGA output was generated using Scanpy v.1.4.3 (40) with default values and a threshold of 0.15.

TCR analysis

TCR-seq data for each sample were processed using Cell Ranger software (versions as above), with the command “cellranger vdj” using the human reference genome GRCh38.

Statistical analysis

All flow cytometry experiments were analyzed using Prism 8 (GraphPad software, version 8.4.2). All data were presented as means \pm SEM. Statistical differences were assessed using two-way analysis of variance (ANOVA) test or two-tailed paired Student's *t* test.

SUPPLEMENTARY MATERIALS

immunology.sciencemag.org/cgi/content/full/6/55/eabd5778/DC1

Materials and Methods

Fig. S1. Comparison of the 3' versus 5' single-cell chemistries and general characterization of total CD3⁺ T cell subsets.

Fig. S2. Gene signatures and biological pathways differentiating precursors and terminally differentiated CD8⁺ T cells.

Fig. S3. Flow cytometry gating strategy and quantification of silhouette score and maximum prediction score of the label transfer method in CD8⁺ T cell subsets.

Fig. S4. Quantification of shared clones among the CD8⁺ clusters and transition index.

Fig. S5. Characterization of the cycling CD8⁺ T cells.

Fig. S6. Analysis of tissue specificity of tumor, juxtatumor, and blood tissue in patients with NSCLC.

Table S1. Clinical data.

Table S2. Differentially expressed genes per cluster.

Table S3. Gene signatures.

Table S4. TCR information.

Table S5. Raw data table.

[View/request a protocol for this paper from Bio-protocol.](#)

REFERENCES AND NOTES

- R. S. Herbst, J. V. Heymach, S. M. Lippman, Lung cancer. *N. Engl. J. Med.* **359**, 1367–1380 (2008).
- E. Brambilla, G. Le Teuff, S. Marguet, S. Lantuejoul, A. Dunant, S. Graziano, R. Pirker, J.-Y. Douillard, T. Le Chevalier, M. Filipits, R. Rosell, R. Kratzke, H. Popper, J.-C. Soria, F. A. Shepherd, L. Seymour, M. S. Tsao, Prognostic effect of tumor lymphocytic infiltration in resectable non-small-cell lung cancer. *J. Clin. Oncol.* **34**, 1223–1230 (2016).
- A. Uryvaev, M. Pashak, D. Hershkovits, E. Sabo, G. Bar-Sela, The role of tumor-infiltrating lymphocytes (TILs) as a predictive biomarker of response to anti-PD1 therapy in patients with metastatic non-small cell lung cancer or metastatic melanoma. *Med. Oncol.* **35**, 25 (2018).
- S. L. Topalian, C. G. Drake, D. M. Pardoll, Immune checkpoint blockade: A common denominator approach to cancer therapy. *Cancer Cell* **27**, 450–461 (2015).
- P. Sharma, J. P. Allison, Immune checkpoint targeting in cancer therapy: Toward combination strategies with curative potential. *Cell* **161**, 205–214 (2015).
- M. A. Paley, D. C. Kroy, P. M. Odorizzi, J. B. Johnnidis, D. V. Dolfi, B. E. Barnett, E. K. Bikoff, E. J. Robertson, G. M. Lauer, S. L. Reiner, E. J. Wherry, Progenitor and terminal subsets of CD8⁺ T cells cooperate to contain chronic viral infection. *Science* **338**, 1220–1225 (2012).
- D. T. Utzschneider, M. Charmoy, V. Chennupati, L. Pousse, D. P. Ferreira, S. Calderon-Copete, M. Danilo, F. Alfei, M. Hofmann, D. Wieland, S. Pradervand, R. Thimme, D. Zehn, W. Held, T cell factor 1-expressing memory-like CD8⁺ T cells sustain the immune response to chronic viral infections. *Immunity* **45**, 415–427 (2016).
- Z. Chen, Z. Ji, S. F. Ngiew, S. Manne, Z. Cai, A. C. Huang, J. Johnson, R. P. Staube, B. Bengsch, C. Xu, S. Yu, M. Kurachi, R. S. Herati, L. A. Vella, A. E. Baxter, J. E. Wu, O. Khan, J.-C. Beltra, J. R. Giles, E. Stelekati, L. M. McLane, C. W. Lau, X. Yang, S. L. Berger, G. Vahedi, H. Ji, E. J. Wherry, TCF-1-centered transcriptional network drives an effector versus exhausted CD8 T cell-fate decision. *Immunity* **51**, 840–855.e5 (2019).
- S. J. Im, M. Hashimoto, M. Y. Gerner, J. Lee, H. T. Kissick, M. C. Burger, Q. Shan, J. S. Hale, J. Lee, T. H. Nasti, A. H. Sharpe, G. J. Freeman, R. N. Germain, H. I. Nakaya, H.-H. Xue, R. Ahmed, Defining CD8⁺ T cells that provide the proliferative burst after PD-1 therapy. *Nature* **537**, 417–421 (2016).
- C. U. Blank, W. N. Haining, W. Held, P. G. Hogan, A. Kallies, E. Lugli, R. C. Lynn, M. Philip, A. Rao, N. P. Restifo, A. Schietinger, T. N. Schumacher, P. L. Schwartzberg, A. H. Sharpe, D. E. Speiser, E. J. Wherry, B. A. Youngblood, D. Zehn, Defining ‘T cell exhaustion’. *Nat. Rev. Immunol.* **19**, 665–674 (2019).
- E. J. Wherry, T cell exhaustion. *Nat. Immunol.* **12**, 492–499 (2011).
- D. S. Thommen, V. H. Koelzer, P. Herzig, A. Roller, M. Trefny, S. Dimeloe, A. Kiialainen, J. Hanhart, C. Schill, C. Hess, S. S. Prince, M. Wiese, D. Lardinois, P.-C. Ho, C. Klein, V. Karanikas, K. D. Mertz, T. N. Schumacher, A. Zippelius, A transcriptionally and functionally distinct PD-1⁺ CD8⁺ T cell pool with predictive potential in non-small-cell lung cancer treated with PD-1 blockade. *Nat. Med.* **24**, 994–1004 (2018).
- X. Guo, Y. Zhang, L. Zheng, C. Zheng, J. Song, Q. Zhang, B. Kang, Z. Liu, L. Jin, R. Xing, R. Gao, L. Zhang, M. Dong, X. Hu, X. Ren, D. Kirchhoff, H. G. Roeder, T. Yan, Z. Zhang, Global characterization of T cells in non-small-cell lung cancer by single-cell sequencing. *Nat. Med.* **24**, 978–985 (2018).
- H. Li, A. M. van der Leun, I. Yofe, Y. Lubling, D. Gelbard-Solodkin, A. C. J. van Akkooi, M. van den Braber, E. A. Rozeman, J. B. A. G. Haanen, C. U. Blank, H. M. Horlings, E. David, Y. Baran, A. Bercovich, A. Lifshitz, T. N. Schumacher, A. Tanay, I. Amit, Dysfunctional CD8 T cells form a proliferative, dynamically regulated compartment within human melanoma. *Cell* **176**, 775–789.e18 (2019).
- C. Zheng, L. Zheng, J.-K. Yoo, H. Guo, Y. Zhang, X. Guo, B. Kang, R. Hu, J. Y. Huang, Q. Zhang, Z. Liu, M. Dong, X. Hu, W. Ouyang, J. Peng, Z. Zhang, Landscape of infiltrating T cells in liver cancer revealed by single-cell sequencing. *Cell* **169**, 1342–1356.e16 (2017).
- E. Azizi, A. J. Carr, G. Plitas, A. E. Cornish, C. Konopacki, S. Prabhakaran, J. Nainys, K. Wu, V. Kiseliovas, M. Setty, K. Choi, R. M. Fromme, P. Dao, P. T. McKenney, R. C. Wasti, K. Kadaveru, L. Mazutis, A. Y. Rudensky, D. Pe'er, Single-cell map of diverse immune phenotypes driven by the tumor microenvironment. *Cell* **174**, 1293–1308.e36 (2018).
- M. Sade-Feldman, K. Yizhak, S. L. Bjorgaard, J. P. Ray, C. G. de Boer, R. W. Jenkins, D. J. Lieb, J. H. Chen, D. T. Frederick, M. Barzily-Rokni, S. S. Freeman, A. Reuben, P. J. Hoover, A.-C. Villani, E. Ivanova, A. Portell, P. H. Lizotte, A. R. Aref, J.-P. Eliane, M. R. Hammond, H. Vitzthum, S. M. Blackmon, B. Li, V. Gopalakrishnan, S. M. Reddy, Z. A. Cooper, C. P. Pawletz, D. A. Barbie, A. Stemmer-Rachamimov, K. T. Flaherty, J. A. Wargo, G. M. Boland, R. J. Sullivan, G. Getz, N. Hacohen, Defining T cell states associated with response to checkpoint immunotherapy in melanoma. *Cell* **175**, 998–1013.e20 (2018).
- T. Stuart, A. Butler, P. Hoffman, C. Hafemeister, E. Papalexi, W. M. Mauck III, Y. Hao, M. Stoekius, P. Smibert, R. Satija, Comprehensive integration of single-cell data. *Cell* **177**, 1888–1902.e21 (2019).
- B. C. Miller, D. R. Sen, R. Al Aboosy, K. Bi, Y. V. Virkud, M. W. LaFleur, K. B. Yates, A. Lako, K. Felt, G. S. Naik, M. Manos, E. Gjini, J. R. Kuchroo, J. J. Ishizuka, J. L. Collier, G. K. Griffin, S. Maleri, D. E. Comstock, S. A. Weiss, F. D. Brown, A. Panda, M. D. Zimmer, R. T. Manguso, F. S. Hodi, S. J. Rodig, A. H. Sharpe, W. N. Haining, Subsets of exhausted CD8⁺ T cells differentially mediate tumor control and respond to checkpoint blockade. *Nat. Immunol.* **20**, 326–336 (2019).
- L. Pace, C. Goudot, E. Zueva, P. Gueguen, N. Burgdorf, J. J. Waterfall, J.-P. Quivy, G. Almozuni, S. Amigorena, The epigenetic control of stemness in CD8⁺ T cell fate commitment. *Science* **359**, 177–186 (2018).
- P. A. Szabo, H. M. Levitin, M. Miron, M. E. Snyder, T. Senda, J. Yuan, Y. L. Cheng, E. C. Bush, P. Dogra, P. Thapa, D. L. Farber, P. A. Sims, Single-cell transcriptomics of human T cells reveals tissue and activation signatures in health and disease. *Nat. Commun.* **10**, 4706 (2019).
- D. Zemmour, R. Zilionis, E. Kiner, A. M. Klein, D. Mathis, C. Benoist, Single-cell gene expression reveals a landscape of regulatory T cell phenotypes shaped by the TCR. *Nat. Immunol.* **19**, 291–301 (2018).
- S. J. Marciniak, C. Y. Yun, S. Oyadomari, I. Novoa, Y. Zhang, R. Jungreis, K. Nagata, H. P. Harding, D. Ron, CHOP induces death by promoting protein synthesis and oxidation in the stressed endoplasmic reticulum. *Genes Dev.* **18**, 3066–3077 (2004).
- I. Tirosh, B. Izar, S. M. Prakadan, M. H. Wadsworth II, D. Treacy, J. J. Trombetta, A. Rotem, C. Rodman, C. Lian, G. Murphy, M. Fallahi-Sichani, K. Dutton-Regester, J.-R. Lin, O. Cohen, P. Shah, D. Lu, A. S. Genshaft, T. K. Hughes, C. G. K. Ziegler, S. W. Kazer, A. Gaillard, K. E. Kolb, A.-C. Villani, C. M. Johannessen, A. Y. Andreev, E. M. Van Allen, M. Bertagnoli, P. K. Sorger, R. J. Sullivan, K. T. Flaherty, D. T. Frederick, J. Jané-Valbuena, C. H. Yoon, O. Rozenblatt-Rosen, A. K. Shalek, A. Regev, L. A. Garraway, Dissecting the multicellular ecosystem of metastatic melanoma by single-cell RNA-seq. *Science* **352**, 189–196 (2016).
- N. A. M. Kragten, F. M. Behr, F. A. Vieira Braga, E. B. M. Remmerswaal, T. H. Wesselink, A. E. Oja, P. Hombrink, A. Kallies, R. A. W. van Lier, R. Stark, K. P. J. M. van Gisbergen, Blimp-1 induces and Hobit maintains the cytotoxic mediator granzyme B in CD8 T cells. *Eur. J. Immunol.* **48**, 1644–1662 (2018).
- A.-P. Ganesan, J. Clarke, O. Wood, E. M. Garrido-Martin, S. J. Chee, T. Mellows, D. Samaniego-Castruita, D. Singh, G. Seumois, A. Alzetani, E. Woo, P. S. Friedmann,

- E. V. King, G. J. Thomas, T. Sanchez-Elsner, P. Vijayanand, C. H. Ottensmeier, Tissue-resident memory features are linked to the magnitude of cytotoxic T cell responses in human lung cancer. *Nat. Immunol.* **18**, 940–950 (2017).
27. J. Clarke, B. Panwar, A. Madrigal, D. Singh, R. Gujar, O. Wood, S. J. Chee, S. Eschweiler, E. V. King, A. S. Awad, C. J. Hanley, K. J. McCann, S. Bhattacharyya, E. Woo, A. Alzetani, G. Seumois, G. J. Thomas, A.-P. Ganesan, P. S. Friedmann, T. Sanchez-Elsner, F. Ay, C. H. Ottensmeier, P. Vijayanand, Single-cell transcriptomic analysis of tissue-resident memory T cells in human lung cancer. *J. Exp. Med.* **216**, 2128–2149 (2019).
28. T. Duhén, R. Duhén, R. Montler, J. Moses, T. Moudgil, N. F. de Miranda, C. P. Goodall, T. C. Blair, B. A. Fox, J. E. McDermott, S.-C. Chang, G. Grunkemeier, R. Leidner, R. B. Bell, A. D. Weinberg, Co-expression of CD39 and CD103 identifies tumor-reactive CD8⁺ T cells in human solid tumors. *Nat. Commun.* **9**, 2724 (2018).
29. K. E. Yost, A. T. Satpathy, D. K. Wells, Y. Qi, C. Wang, R. Kageyama, K. L. McNamara, J. M. Granja, K. Y. Sarin, R. A. Brown, R. K. Gupta, C. Curtis, S. L. Bucktrout, M. M. Davis, A. L. S. Chang, H. Y. Chang, Clonal replacement of tumor-specific T cells following PD-1 blockade. *Nat. Med.* **25**, 1251–1259 (2019).
30. A. Leruste, J. Tosello, R. N. Ramos, A. Tauziède-Espariat, S. Brohard, Z.-Y. Han, K. Beccaria, M. Andrianteranagna, P. Caudana, J. Nikolic, C. Chauvin, L. L. Niborski, V. Manriquez, W. Richer, J. Masliah-Planchon, S. Grossetête-Lalami, M. Bohec, S. Lameiras, S. Baulande, C. Pouponnot, A. Coulomb, L. Galmiche, D. Surdez, N. Servant, J. Helft, C. Sedlik, S. Puget, P. Benaroch, O. Delattre, J. J. Waterfall, E. Piaggio, F. Bourdeaut, Clonally expanded T cells reveal immunogenicity of rhabdoid tumors. *Cancer Cell* **36**, 597–612.e8 (2019).
31. T. Dupic, Q. Marcou, A. M. Walczak, T. Mora, Genesis of the $\alpha\beta$ T-cell receptor. *PLoS Comput. Biol.* **15**, e1006874 (2019).
32. Y. Elhanati, Z. Sethna, C. G. Callan Jr., T. Mora, A. M. Walczak, Predicting the spectrum of TCR repertoire sharing with a data-driven model of recombination. *Immunol. Rev.* **284**, 167–179 (2018).
33. L. Zhang, X. Yu, L. Zheng, Y. Zhang, Y. Li, Q. Fang, R. Gao, B. Kang, Q. Zhang, J. Y. Huang, H. Konno, X. Guo, Y. Ye, S. Gao, S. Wang, X. Hu, X. Ren, Z. Shen, W. Ouyang, Z. Zhang, Lineage tracking reveals dynamic relationships of T cells in colorectal cancer. *Nature* **564**, 268–272 (2018).
34. A. M. van der Leun, D. S. Thommen, T. N. Schumacher, CD8⁺ T cell states in human cancer: Insights from single-cell analysis. *Nat. Rev. Cancer* **20**, 218–232 (2020).
35. J. B. Andersen, Single cell profiling reveals window for immunotherapy in liver cancers. *Hepatobil. Surg. Nutr.* **7**, 48–51 (2018).
36. W. H. Hudson, J. Gensheimer, M. Hashimoto, A. Wieland, R. M. Valanparambil, P. Li, J.-X. Lin, B. T. Konieczny, S. J. Im, G. J. Freeman, W. J. Leonard, H. T. Kissick, R. Ahmed, Proliferating transitory T cells with an effector-like transcriptional signature emerge from PD-1⁺ stem-like CD8⁺ T cells during chronic infection. *Immunity* **51**, 1043–1058.e4 (2019).
37. A. Petrelli, G. Mijnheer, D. P. H. van Konijnenburg, M. M. van der Wal, B. Giovannone, E. Mocholi, N. Vazirpanah, J. C. Broen, D. Hijnen, B. Oldenburg, P. J. Coffey, S. J. Vastert, B. J. Prakken, E. Spierings, A. Pandit, M. Mokry, F. van Wijk, PD-1⁺ CD8⁺ T cells are clonally expanding effectors in human chronic inflammation. *J. Clin. Invest.* **128**, 4669–4681 (2018).
38. J.-C. Beltra, S. Manne, M. S. Abdel-Hakeem, M. Kurachi, J. R. Giles, Z. Chen, V. Casella, S. F. Ngjow, O. Khan, Y. J. Huang, P. Yan, K. Nzingha, W. Xu, R. K. Amaravadi, X. Xu, G. C. Karakousis, T. C. Mitchell, L. M. Schuchter, A. C. Huang, E. J. Wherry, Developmental relationships of four exhausted CD8⁺ T cell subsets reveals underlying transcriptional and epigenetic landscape control mechanisms. *Immunity* **52**, 825–841.e8 (2020).
39. Y. Zhou, B. Zhou, L. Pache, M. Chang, A. H. Khodabakhshi, O. Tanaseichuk, C. Benner, S. K. Chanda, Metascope provides a biologist-oriented resource for the analysis of systems-level datasets. *Nat. Commun.* **10**, 1523 (2019).
40. F. A. Wolf, P. Angerer, F. J. Theis, SCANPY: Large-scale single-cell gene expression data analysis. *Genome Biol.* **19**, 15 (2018).

Acknowledgments: We wish to thank the flow cytometry platform of Institut Curie and L. Guyonnet for helpful discussions. We thank W. Richer for fruitful discussions on label transfer and TCR analyses. We thank all the thoracic surgery, respiratory medicine, pathology, and tissue procurement staff of Institut Mutualiste Montsouris, as well as all the patients and their families. **Funding:** C.M. received a PhD fellowship from Servier Laboratories and funds by the PhD program “FIRE - Programme Bettencourt”. P.G. is supported by a PhD fellowship from Ligue Nationale contre le Cancer at Université Paris Descartes (Paris V). This study was supported by grants from “Janssen Horizon,” “Fondation ARC pour la recherche sur le cancer,” “Fondation chercheur et trouver,” “European Research Council COG 724208” (T.D., T.M. and A.M.W.), LabEx DCBIOL (ANR-10-IDEX-0001-02 PSL and ANR-11-LABX-0043), Center of Clinical Investigation (CIC IGR-Curie 1428), Equipex (ANR-10-EQPX-03), France Génomique Consortium (ANR-10-INBS-09-08) from the Agence Nationale de la Recherche (“Investissements d’Avenir” program), and the SIRIC-Curie program (SIRIC grant INCa-DGOS- 4654) (J.J.W.). **Author contributions:** S.A., J.J.W., and O.L. conceived the project. C.M. and M.L. designed and performed experiments and acquired the data. P.G. and C.M. analyzed and interpreted the data. T.D. analyzed the data. T.M., A.M.W., C.G., J.J.W., and S.A. guided computational analysis. S.B. and S.L. were involved in data acquisition. N.G., A.S.-G., and M.L. were involved in patient inclusion and sample acquisition. C.M., P.G., J.J.W., and S.A. wrote the manuscript with contributions from all authors. J.J.W. and S.A. supervised the project. **Competing interests:** The authors declare that they have no competing interests. **Data and materials availability:** The data for this study are being deposited in the Gene Expression Omnibus database (GSE1162500). Code used to analyze the data is available at https://github.com/p-gueguen/single_cell_NSCLC.

Submitted 6 July 2020
Accepted 23 December 2020
Published 29 January 2021
10.1126/sciimmunol.abd5778

Citation: P. Gueguen, C. Metoikidou, T. Dupic, M. Lawand, C. Goudot, S. Baulande, S. Lameiras, O. Lantz, N. Girard, A. Seguin-Givelet, M. Lefevre, T. Mora, A. M. Walczak, J. J. Waterfall, S. Amigorena, Contribution of resident and circulating precursors to tumor-infiltrating CD8⁺ T cell populations in lung cancer. *Sci. Immunol.* **6**, eabd5778 (2021).

Contribution of resident and circulating precursors to tumor-infiltrating CD8⁺ T cell populations in lung cancer

Paul Gueguen, Christina Metoikidou, Thomas Dupic, Myriam Lawand, Christel Goudot, Sylvain Baulande, Sonia Lameiras, Olivier Lantz, Nicolas Girard, Agathe Seguin-Givelet, Marine Lefevre, Thierry Mora, Aleksandra M. Walczak, Joshua J. Waterfall and Sebastian Amigorena

Sci. Immunol. **6**, eabd5778.
DOI: 10.1126/sciimmunol.abd5778

Tumor-infiltrating lymphocyte lessons

The presence of intratumoral CD8⁺ tumor-infiltrating lymphocytes (TILs) is associated with better outcomes for patients with non–small cell lung cancer (NSCLC). These TILs consist of multiple subpopulations, and Gueguen *et al.* use single-cell RNA and T cell receptor sequencing to examine the origins and functional organization of TILs in NSCLC. They identified two precursor CD8⁺ TIL subpopulations with memory-like gene signatures. One of these subpopulations is detected in peripheral blood, whereas the other population is detected in juxtatumor tissue. Both subsets differentiate through a similar transitional stage into terminal effector TILs, which appear to be actively cycling within the tumor. Together, these results better define the origins and differentiation of CD8⁺ TILs associated with NSCLC.

ARTICLE TOOLS

<http://immunology.sciencemag.org/content/6/55/eabd5778>

SUPPLEMENTARY MATERIALS

<http://immunology.sciencemag.org/content/suppl/2021/01/25/6.55.eabd5778.DC1>

REFERENCES

This article cites 40 articles, 6 of which you can access for free
<http://immunology.sciencemag.org/content/6/55/eabd5778#BIBL>

PERMISSIONS

<http://www.sciencemag.org/help/reprints-and-permissions>

Use of this article is subject to the [Terms of Service](#)

Science Immunology (ISSN 2470-9468) is published by the American Association for the Advancement of Science, 1200 New York Avenue NW, Washington, DC 20005. The title *Science Immunology* is a registered trademark of AAAS.

Copyright © 2021 The Authors, some rights reserved; exclusive licensee American Association for the Advancement of Science. No claim to original U.S. Government Works